Kallunki, J.

Complex Type II Solar Radio Event on 4 July 2022

Published in:
Latvian Journal of Physics and Technical Sciences

DOI:
10.2478/lpts-2022-0044

Published: 01/12/2022

Document Version
Publisher's PDF, also known as Version of record

sciendo

LATVIAN JOURNAL OF PHYSICS
AND TECHNICAL SCIENCES
2022, N 6

DOI: 10.2478/lpts-2022-0044

COMPLEX TYPE II SOLAR RADIO EVENT ON 4 JULY 2022

J. Kallunki

Aalto University,
Metsähovi Radio Observatory, Finland
*e-mail: juha.kallunki@aalto.fi

On 4 July 2022, a complex low-frequency solar radio burst was observed in Metsähovi Radio Observatory of Aalto University. The radio burst was observed at a frequency range between 20 and 80 MHz. In GOES (Geostationary Operational Environmental Satellite) class, the event was classified as C5.1. However, coronal mass ejection (CME) was not associated to this event. The observed radio burst was a long-lasting (~10 minutes) event, and it could be mainly classified as type II solar radio event. Also type III solar events were observed before long-lasting type II event. The event includes common frequency drifting emission structures, both fundamental and harmonic structures, but also rarely observed continuum-like or stationary structure. It is assumed that the continuum-like radio emission structure is originated from the stationary flare (coronal) loop, which was visible over the whole event. The drifting emission structure means accelerated electrons, which are produced by the shock related phenomena. The paper provides the observations from this event on radio wavelength, and also soft-X-ray regime and optical wavelength (AIA 171). In addition, a possible, simplified scenario is presented for forming the drifting and continuum solar radio emissions in type II solar burst.

Keywords: *Radio astronomy, solar activity, solar radio emission, type II solar radio burst.*

1. INTRODUCTION

Low-frequency (< 100 MHz) solar radio bursts have been studied for decades. They have a major role in the space weather investigations since they originate in the same layers of the solar atmosphere in which geo-effective disturbances originate [1]. The radio bursts can be classified based on how they appear in dynamic spectrum, e.g., based on their duration and frequency drift. The most common types of radio bursts are: I, II, III, IV and V. Other more complex bursts are also possible, which are not matching directly with I–IV classifications. Type II solar radio bursts have long been linked to solar eruptive events such as coronal mass ejections (CMEs), also they have been linked to the flare blast shock waves. Type II solar radio emission often occurs after the lift-off of the CME [2]. It has also been reported that emission steps of type II radio burst are the following: (1) the acceleration of electrons by the shock, (2) the excitation of Langmuir waves by the energetic electrons by streaming instabilities, and (3) the conversion of Langmuir waves into escaping radiation at the fundamental (*F*) and second harmonic (*H*) of the electron plasma frequency (f_{pe}) [3]. Both drifting and continuum-like emission structures have been detected in touch with type II bursts. The drifting structures are related to moving shocks. The stationary emission is forming at the stage when the CME causes the streamer to expand quickly locally [4]. In addition, type II solar radio bursts typically occur at around the time of the soft X–ray peak [1]. Solar type III radio bursts result from impulsively accelerated electrons. Their radio emission is drifting fast from higher to lower frequencies [4], [5].

Type II solar radio bursts, which have a continuum-like or stationary emission structure, have been reported earlier, e.g., [6]–[8]. However, these events are not very common. Most of the type II radio events have a drifting emission structure. Previously reported events have had clear relation to CMEs. However, this event had not any connection to CME. This article presents and analyses a complex low-frequency solar radio event, which has both drifting and continuum-like emission structures. The complex low-frequency (<100 MHz) solar radio event was observed on 4 July 2022. The radio observations were made at Metsähovi Radio Observatory (MRO) of Aalto University.

2. INSTRUMENTATION

Metsähovi Radio Observatory (MRO) of Aalto University, located in southern Finland (GPS coordinates: N 60:13.04, E 24:23.35), installed a crossed-dipole antenna (CDA) manufactured by Reeve Observatory in October 2017. The new antenna, dubbed the Metsähovi Solar Observing Low-frequency Antenna METSOLA, has frequency coverage between 18 MHz and 90 MHz. The antenna has two different polarization outputs (east–west and north–south), which makes it possible to study also the polarization properties of solar flares. The Sun is rather vactive at frequencies below 100 MHz even if the solar activity phase is low. On the other hand, one of the main challenges when making radio astronomical observations on lower fre-

quencies ($f \simeq 100$ MHz) is radio frequency interference (RFI). This frequency range is allocated for various services such as broadcasting, amateur and mobile. However, it has been found that the observing band between approximately 30 and 80 MHz was still reasonably free from interferences and usable for solar observations [9], [10]. Figure 1 shows METSOLA instrument.

In 2021, the noise calibration was added to the system (east–west polarization). This makes it possible to estimate the flux density of the observed radio bursts. The flux density estimation method is described more carefully in [11]. In this study, the time and frequency profiles of the observed solar radio burst were studied; thus, there was no need for the accurate flux calibration.

Fig. 1. METSOLA instrument installed in Metsähovi Radio Observatory of Aalto University.

3. OVERVIEW OF OBSERVATIONS

On 4 June 2022, a complex solar type II radio burst was observed, starting at 13:35 UT, which had both drifting and stationary or continuum-like structures, which was preceded by type III solar event (starting at 13:34 UT). The event was observed at a frequency range between 20 and 85 MHz. The radio data were obtained with the radio telescopes of Metsähovi Radio Observatory of Aalto University. In GOES class, the event was classified as C5.1. However, CME was not associated to this event. Near the soft-X-ray peak (0.1–0.8 nm), type III solar burst was detected. The soft-X-ray peak was at 13:31 UT (0.05-0.4 nm) and 13:33 UT (0.1–0.8 nm), marked with a red dashed line in Fig. 2.

Type II solar radio burst started (~13:34:20 UT) with the drifting structure; both fundamental (F) and harmonic (H) emissions could be detected. A minute after that, stationary or continuum-like emission structure was starting (at 13:35:30 UT) at frequencies between ~45 and 48 MHz, marked with a green dashed line in Fig. 1. The stationary emission went until 13:41 UT, which was followed by three different drifting structures (type II solar burst). The event was recorded with two different polarizations (east–west and north–south) using METSOLA instrument. No significant differences in measurements between the linear polarizations were noted in this case. Figure 2 shows the dynamic spectra of the observed low-frequency solar radio event.

Figure 3 shows the GOES soft-X-ray flux on this event. The soft-X-ray flux peaked (0.1–0.8 nm) about one minute before the first type III solar burst. Figure 4 presents the solar radio map at 37 GHz, which was observed around after two hours when the event started. The radio map was observed with MRO 14-metre radio telescope. An area marked with a blue arrow shows the active regions, which produced the radio burst presented here. The maximum radio brightness intensity is 105.75 % of the QSL (8570 K).

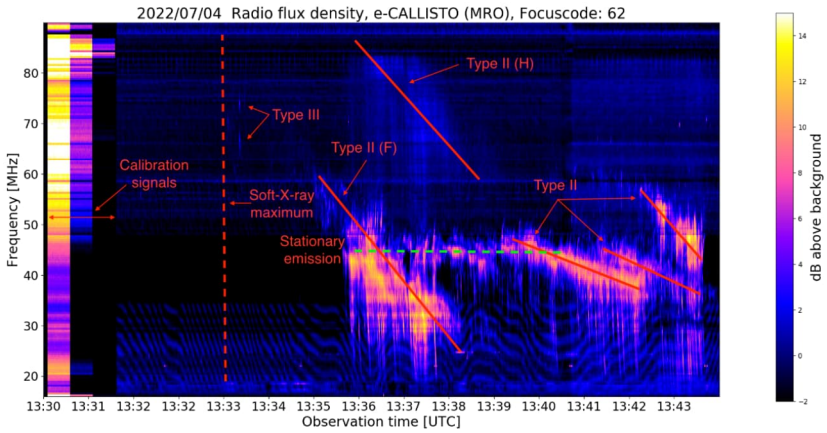

Fig. 2. A complex low-frequency (20–90 MHz) solar event observed on 4 June 2022.
A wavy signal, which is observed over the whole-time range, is a sign of RFI (Radio Frequency Interference).

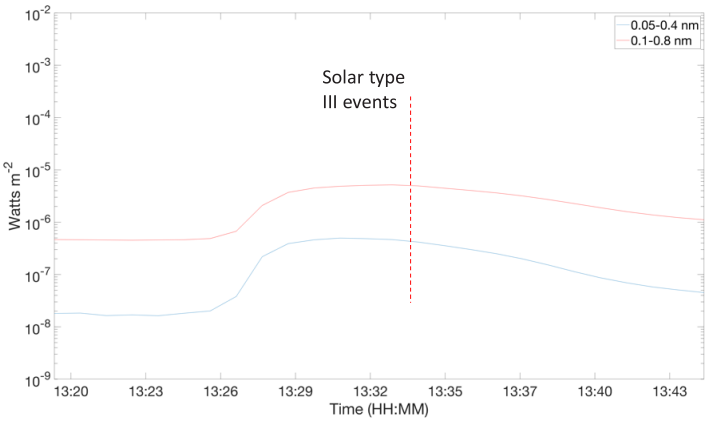

Fig. 3. The soft-X-ray flux in the period of the solar radio event. The soft-X-ray event peaks close (approximately with a one-minute difference) to first type III solar burst. The red dashed line indicates the starting time of type III solar burst.

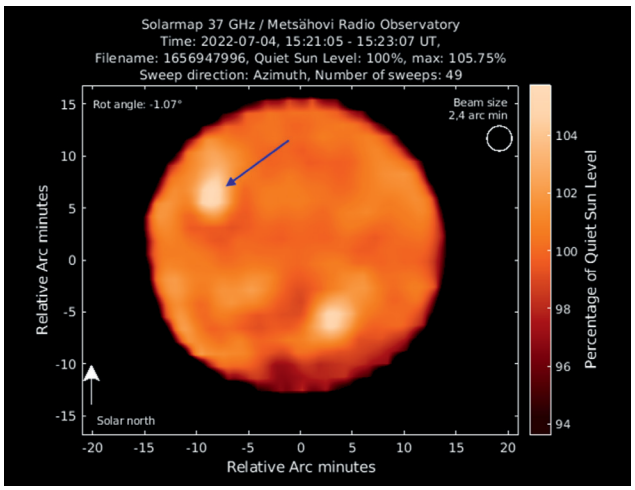

Fig. 4. The radio map at 37 GHz, observed at 15:21:05 UT. The blue arrow shows a region, which was an origin of complex solar burst. The map was observed roughly after two hours after the burst occurred.

The observed solar radio map also indicates the fact that the event was relatively weak; thus, the brightness temperature of the active region after two hours from the event was already rather low (105.75 % of the QSL).

In addition, Figure 4 shows SDO/AIA 171 Å seven maps over the radio event occurring period. This wavelength, 171 Å, shows the quiet corona and coronal loops. A larger active region stays stabile over the radio event. However, some smaller flaring region, marked with a red arrow, is visible. This region is located closer to the footpoint of the coronal loop. This flaring region was visible at ~13:32:30 UT, when soft-X-ray peaked. In addition, the flaring region was visible between 13:36:45 UT and 13:42:45 UT. The size of this smaller flaring region was as the largest at 13:36:45 UT. At 13:42:45 UT, the region was barely visible anymore. The coronal (flare) loops were visible over the whole period, and they were rather stable.

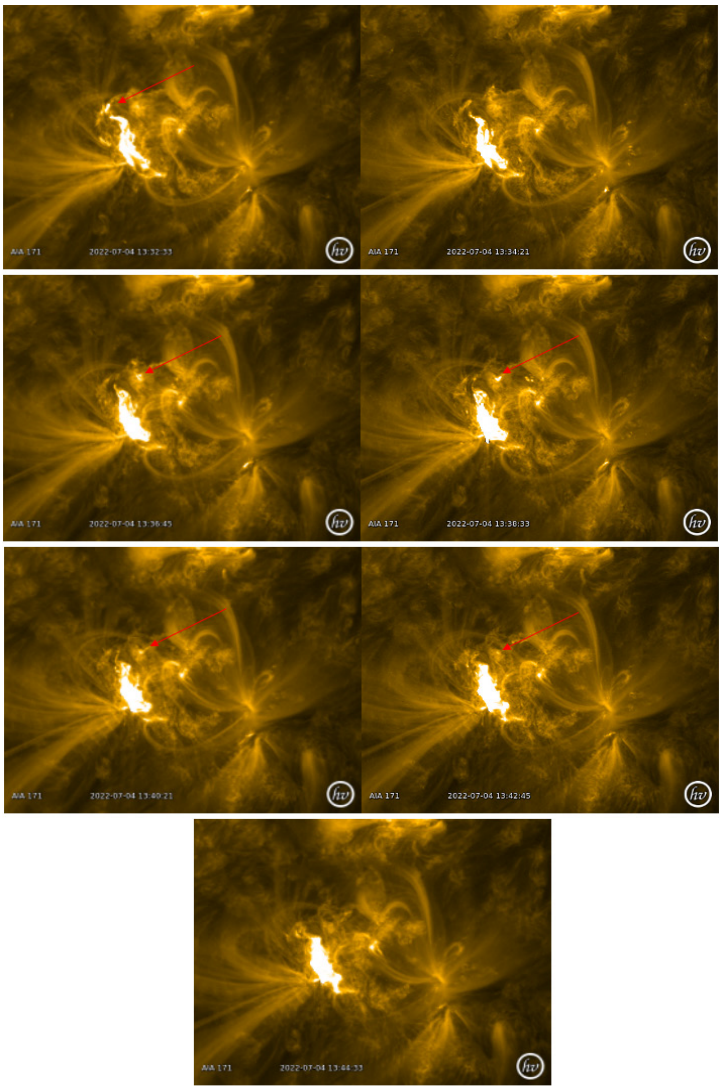

Fig. 5. Seven SDO/AIA (171 Å) maps, which show the variation of the flaring region. Red arrows show the location of a smaller flaring region in the footpoint of the flare loop.

a. Drift Rates of Radio Bursts

The drifting rate (D) was defined for each burst structure, according to Eq. (1). The upper observing range of the instrument is 90 MHz; thus, the upper frequency band of harmonic type II solar burst could not be observed. Besides, the real upper observing limit was 85 MHz due to prevailing RFI environment.

$$D = \frac{df}{dt} = \frac{f_1 - f_0}{t_1 - t_0}, \quad (1)$$

where f_0 and f_1 are the frequency of the burst at start (t_0) and end (t_1) of the observed burst, respectively. Table 1 presents the drift rates for each burst structure. In Table 1, F indicates fundamental structure and H fundamental structure, respectively.

Table 1. The Drift Rates for Each Burst Structure

Starting time (UT)	Drift rate (MHz s^{-1})	Burst type
13:34:20	-2.89	Type III
13:36:00	-0.17	Type II (F)
13:36:50	-0.16	Type II (H)
13:38:58	-0.08	Type II
13:40:13	-0.06	Type II
13:43:16	-0.17	Type II

After continuum structure, three drifting structures were followed. The drift rate of two first bursts was smaller than the third one. The drift rate of the third burst was consistent with the first type II solar burst. The result was consistent with earlier observation, e.g., [12], [13], where the observed drift rates varied between 0.44 MHz/s and 12 MHz/s for type III solar bursts, and for type II burst frequency drift was at the rate of ~0.14 MHz s^{-1} [4], respectively. It can be conclude that the observed drift rates match accurately with those previously reported. The propagation height of the continuum emission can also be estimated using the Newkirk 1st-order atmospheric density model, e.g., [9].

$$n_e = n_0 \times 10^{4.32\frac{R_\odot}{R}}, \quad (2)$$

where R is distance from the solar centre, $R_\odot$ is the solar radius, n_0 is 4.2×10^4 cm^{-1} and n_e is electron density on certain height on the solar atmosphere. The connection between the plasma frequency (v_{pe}) and the electron density (n_e) can be estimated as follows [e.g., 14]:

$$v_{pe} \approx 9000 \times \sqrt{n_e}. \quad (3)$$

Frequencies 45 and 48 MHz correspond to propagation distances 1.52 $R_\odot$ and 1.55 $R_\odot$, respectively.

4. CONCLUSIONS

Type II solar burst with stationary emission structure has been rarely reported. A majority of type II solar events are drifting structures. The prevailing interpretation is that stationary emission is a signature of the standing shock. Associated with type II solar bursts, the so-called herringbone radio burst are also reported [4]. The herringbone

bursts look like a continuum emission, but they have narrow bandwidth and very rapid frequency drift rate [15].

A jet eruption caused a steamer-puff CME, which produced both the stationary and drifting emission structures in connection with type II solar burst [4]. However, in our case, CME was not detected. In addition, it has been reported that type IV burst or continuum radiation is produced by electrons trapped in stationary or slowly moving coronal loops [2]. SDO/AIA 171 Å maps showed clear stationary coronal (flare) loop structures, which were stable over the whole observing period. Our observations support interpretation that the continuum type II radio emission can also be originated from stationary or slowly moving coronal (flare) loops. The drifting emission comes from the moving plasmoid ejection (e.g., filament), which was also detected in SDO/AIA 171 Å maps (Fig. 5). Figure 6 presents a possible scenario for forming the drifting and continuum solar radio emissions on type II solar radio burst, which has been analysed in this study.

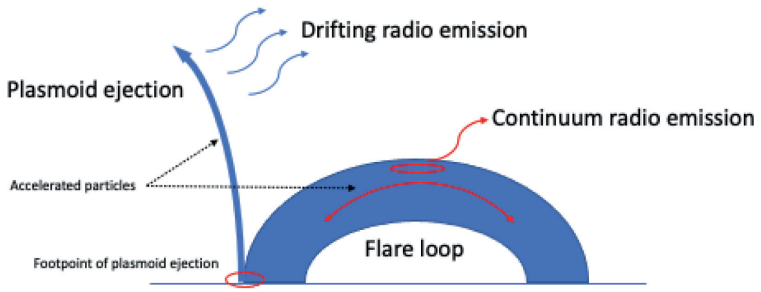

Fig. 6. The proposed, simplified scenario for the formation of the drifting and continuum solar radio emissions in type II solar burst. The drifting radio emission comes from the moving structure and continuum emission comes from flare loop, respectively. It can also be assumed that the radio emission comes from the top of the flare loop.

The drifting structure means that the structure is moving in the solar atmosphere (away from the Sun). The radio emission must be the origin from the structure which is moving. This can mean that emission comes from moving plasmoid ejection. The continuum radio emission means that the structure is not moving in the solar atmosphere. It can then be assumed that emission comes from the flare loop, and more precisely from the top of the flaring loop, since the structure is not moving in the solar atmosphere.

As it has been mentioned, events presented here are very unusual and rare. The model presented in Fig. 6 should be confirmed with other similar events. They will be needed to confirm the findings of the present study. The solar activity is rising constantly, and the maximum of Solar Cycle 25 will reach within the next 2–3 years. This will foretell the rising number of active events, and, hopefully, similar events can be observed within this time frame.

ACKNOWLEDGEMENTS

The HMI data is courtesy of NASA/SDO and the AIA, EVE, and HMI science teams.

REFERENCES

1. White, S. M. (2007). Solar Radio Bursts and Space Weather. *Asian Journal of Physics, 16*, 189–207.
2. Dulk, G. (2001). Solar Radio Emissions. *Planetary Radio Emissions*.
3. Thejappa, G., Zlobec, P., & MacDowall, R. J. (2003). Polarization and Fragmentation of Solar Type II Radio Bursts. *The Astrophysical Journal, 592* (2), 1234–1240. doi:10.1086/375859.
4. Ergun, R. E. (1998). Wind Spacecraft Observations of Solar Impulsive Electron Events Associated with Solar Type III Radio Bursts. *The Astrophysical Journal, 503* (1), 435–445. doi:10.1086/305954.
5. Reid, H. A. S., & Ratcliffe, H. (2014). A Review of Solar Type III Radio Bursts. *Research in Astronomy and Astrophysics, 14* (7), 773–804. doi:10.1088/1674-4527/14/7/003.
6. Chrysaphi, N., Reid, H. A. S., & Kontar, E. P. (2020). First Observation of a Type II Solar Radio Burst Transitioning between a Stationary and Drifting State. *The Astrophysical Journal, 893* (2). doi:10.3847/1538-4357/ab80c1.
7. Aurass, H., & Mann, G. (2004). Radio Observation of Electron Acceleration at Solar Flare Reconnection Outflow Termination Shocks. *The Astrophysical Journal, 615* (1), 526–530. doi:10.1086/424374.
8. Aurass, H., Vršnak, B., & Mann, G. (2002). Shock-Excited Radio Burst from Reconnection Outflow Jet? *Astronomy and Astrophysics, 384*, 273–281. doi:10.1051/0004-6361:20011735.
9. Kallunki, J., McKay, D., & Tornikoski, M. (2021). First Type III Solar Radio Bursts of Solar Cycle 25. *Solar Physics, 296* (4). doi:10.1007/s11207-021-01790-9.
10. Kallunki, J. (2018). Solar Observing System for Radio Frequencies 5–120 MHz. *Astronomische Nachrichten, 339* (656), 656–660. doi:10.1002/asna.201913545.
11. Kallunki, J., Monstein, C., Kirves, P., Tammi, J., & Mujunen, A. (2022). Calibration of CALLISTO data. *Aalto University publication series Science + Technology, 1/2022*. Available at http://urn.fi/URN:ISBN:978-952-64-0795-1
12. Melnik, V. N. (2015). Decameter Type III Bursts with Changing Frequency Drift-Rate Signs. *Solar Physics, (290)* 1, 193–203. doi:10.1007/s11207-014-0577-8.
13. Li, B., Cairns, I. H., & Robinson, P. A. (2011). Effects of Spatial Variations in Electron and Ion Temperatures on Coronal Type III Bursts. *The Astrophysical Journal, 730* (1).
14. Pohjolainen, S., van Driel-Gesztelyi, L., Culhane, J. L., Manoharan, P. K., & Elliott, H. A. (2007). CME Propagation Characteristics from Radio Observations. *Solar Physics, 244* (1–2), 167–188. doi:10.1007/s11207-007-9006-6.
15. Armatas, S. (2019). Detection of Spike-Like Structures Near the Front of Type-II Bursts. *Astronomy and Astrophysics, 624*, A76. doi:10.1051/0004-6361/201834982.